ELSEVIER

Journal of Power Sources 94 (2001) 175–182

JOURNAL OF POWER SOURCES

www.elsevier.com/locate/jpowsour

Preparation of *c*-axis oriented thin films of $LiCoO_2$ by pulsed laser deposition and their electrochemical properties

Yasutoshi Iriyama, Minoru Inaba, Takeshi Abe, Zempachi Ogumi*

Department of Energy & Hydrocarbon Chemistry, Graduate School of Engineering, Kyoto University, Sakyo-ku, Kyoto 606-8501, Japan

Received 26 April 2000; accepted 24 July 2000

Abstract

Thin films of $LiCoO_2$ with a preferred *c*-axis orientation were prepared by pulsed laser deposition. Thin films deposited for 1–2 h had a preferred *c*-axis orientation, but films deposited for 3 h and longer lost the preferred orientation. The textures of these films were investigated in detail by transmission electron microscopy and selected area electron diffraction. The electrochemical properties of these films were compared by cyclic voltammetry and alternating current impedance spectroscopy. In the cyclic voltammograms of the *c*-axis oriented films, the anodic and cathodic peaks corresponding to the first-order phase transition at around 3.9 V were sharp and their peak separation was small due to their thin and uniform texture. However, their smooth surface and texture of the aligned (0 0 3) planes gave a larger charge-transfer resistance and a smaller apparent diffusion coefficient in the direction normal to the substrate, respectively, which resulted in poor utilizations (∼50%) of the active material. The reactivity in the single-phase region at potentials more positive than 4.0 V was lower than that of randomly oriented films.

Keywords: $LiCoO_2$; *c*-Axis orientation; Electrochemical properties; Thin films; Pulsed lazer deposition

1. Introduction

Layered $LiCoO_2$ consists of a close-packed network of oxygen ions with lithium and cobalt ions on alternating (1 1 1) planes of the cubic rock-salt sub-lattice. The edges of CoO_6 octahedra were shared to form CoO_2 sheets, and lithium ions can move in two-dimensional directions between the CoO_2 sheets. $LiCoO_2$ is now being used as a positive electrode material in rechargeable lithium batteries. In commercially available batteries, composite electrodes, which consist of active materials, organic binders, and conductive additives, are used as the positive electrodes, and most of the studies on the positive electrodes have been done using these composite electrodes [1–6]. However, the use of composite electrodes as test samples often leads to difficulties in detailed analysis of their electrochemical lithium insertion/extraction behavior because of their non-uniform potential distributions and unknown electrode surface areas. In order to overcome these problems, thin-film electrodes have been recently fabricated by various methods and their electrochemical properties have been reported [7–10]. For example, Uchida et al. prepared $LiCoO_2$ thin films using a molten carbonate technique and showed that these films had ideal electrochemical properties [7,8]. Bates et al. used radio frequency (RF) magnetron sputtering to prepare $LiCoO_2$ thin films, and developed all solid-state thin-film batteries [9].

As mentioned above, layered $LiCoO_2$ has an anisotropic structure, and thereby electrochemical lithium insertion/extraction behavior must depend strongly on the orientation of the crystal. The use of $LiCoO_2$ thin films with a preferred orientation will give us useful information about the relationship between the orientation of the crystal and the electrochemical behavior. Bates et al. quite recently reported the preparation of (0 0 3) oriented and (1 0 1)–(1 0 4) oriented thin films of $LiCoO_2$, but they did not find clear evidence for the difference in their electrochemical behavior [10].

Pulsed laser deposition (PLD) are becoming a popular tool to prepare thin films of high-temperature superconductors, ferroelectric and ferromagnetic materials, etc. with preferred orientation or epitaxy [11–13]. Using a PLD technique, Antaya et al. prepared layered, spinel, and rock-salt $LiCoO_2$ [14], but did not mentioned about the orientation of their films. We previously reported that *c*-axis oriented films of $LiCoO_2$ can be prepared by PLD [15];

* Corresponding author. Tel.: +81-75-753-4933; fax: +81-75-753-5889.
E-mail address: ogum@scl.kyoto-u.ac.jp (Z. Ogumi).

0378-7753/01/$ – see front matter
PII: S0378-7753(00)00580-2

however, their detailed texture and electrochemical behavior have not been clarified yet. In the present study, we prepared *c*-axis oriented thin films of $LiCoO_2$ by PLD, and investigated in detail their texture by transmission electron microscopy (TEM) and selected area electron diffraction. Their electrochemical properties were studied by cyclic voltammetry and alternating current (ac) impedance spectroscopy. The results were compared with those of randomly oriented thin films.

2. Experimental

Although one of the advantages of PLD is that deposited thin films have compositions close to those of the targets, it is not the case when the targets contain volatile elements and/or have high vapor pressures [16,17]. In the case of lithium-containing materials, the content of lithium in the resulting thin films tends to be lower than that in the targets as reported for $LiNbO_3$ films deposited by PLD [18]. Hence we used a lithium–cobalt-oxide target with a Li/Co ratio greater than unity to compensate the loss of lithium during deposition. The targets were prepared by sintering a mixture of LiOH (Wako Pure Chemical) and $CoCO_3$ (Mitsuwa Pure Chemical) powder with a Li/Co ratio of 1.35 at 1073 K for 24 h under O_2 atmosphere.

PLD was conducted in a vacuum chamber made of stainless steel. A KrF excimer laser (248 nm, Japan Storage Batteries, Model EXL-210) was used as a light source. The laser beam was focused in a 0.02 cm^2 area on the target at an incident angle of 45°. The energy density of the beam was fixed at 2.1 J cm^{-2}, which was measured with a Joule meter (Gentec, EC-500), with a repetition frequency of 10 Hz. The base pressure of the vacuum chamber was $< 5 \times 10^{-3}$ Pa. Oxygen gas was introduced into the chamber and the pressure was maintained at 23 Pa during deposition. Thin films of $LiCoO_2$ were deposited on quartz glass, Pt, and Au substrates heated at 873 K for 1–4 h. The distance between the target and substrate was kept at 40 mm.

Thin films obtained were characterized by scanning electron microscopy (SEM), powder X-ray diffraction (XRD), Raman spectroscopy, and TEM. The fractured cross-sections of thin films deposited on quartz glass substrates were observed by SEM to estimate the thickness and the growth rate. XRD measurements were carried out using a Shimadzu XD-D1 diffractometer equipped with a Cu Kα source. The data were collected in the 2θ range of 2–80° at a scan rate of 0.125° min^{-1}. Raman spectra were recorded using a triple monochromator (Jobin–Yvon, T-64000) with a multi-channel charge-coupled device (CCD) detector. A 514.5 nm line (50 mW) from an argon ion laser (NEC, GLG3280) was used as a light source. TEM observation and selected area electron diffraction were carried out at an accelerating voltage of 200 kV using a Hitachi H-800. For TEM observation, we used special laboratory-made Au micro grids as substrates [19]. Thin films of $LiCoO_2$ were deposited directly on the micro grids, and the films were observed by TEM without any pretreatments.

Electrochemical measurements were carried out using three-electrode cells. The working electrode was the thin film deposited on Pt or Au, which was placed at the bottom of the cell. The surface area of the working electrode was either 0.07 or 0.20 cm^2. The reference and counter electrodes were lithium metal. The electrolyte solution was 1 mol dm^{-3} (M) $LiClO_4$ dissolved in propylene carbonate (Mitsubishi Chemical Co., Battery Grade). The electrochemical behavior of the thin film electrodes was examined by cyclic voltammetry and AC impedance spectroscopy. Cyclic voltammetry was carried out between 3.6 and 4.2 V versus Li/Li^+ at a slow sweep rate of 0.1 mV s^{-1} using an EG&G Princeton Applied Research 273A potentiostat. AC impedance measurements were conducted using a Solartron 1255 frequency response analyzer coupled with the potentiostat. The electrode potential was scanned to a given potential at 0.1 mV s^{-1} and kept at the potential for 20 min. The impedance was then measured by applying a sine wave of 5 mV (rms) amplitude over the frequency range of 10 kHz to 10 mHz. The impedance data were analyzed using a non-liner least squares fitting program (NLLS). All electrochemical measurements were performed at 303 K in an argon-filled glove box.

3. Results and discussion

3.1. Characterization of $LiCoO_2$ thin films

Fig. 1 shows the XRD pattern of a thin film deposited on a quartz glass substrate for 2 h. Only two peaks at $2\theta = 18.95$ and 38.48° were observed, which are indexed as the (0 0 3) and (0 0 6) reflections, respectively, of hexagonal $LiCoO_2$. Other reflections such as (1 0 1), (0 1 2) and (1 0 4), which are usually observed for $LiCoO_2$ powder samples [4], were not observed in the XRD pattern. The absence of reflection lines other than the (0 0 *l*) lines indicated that the film had a

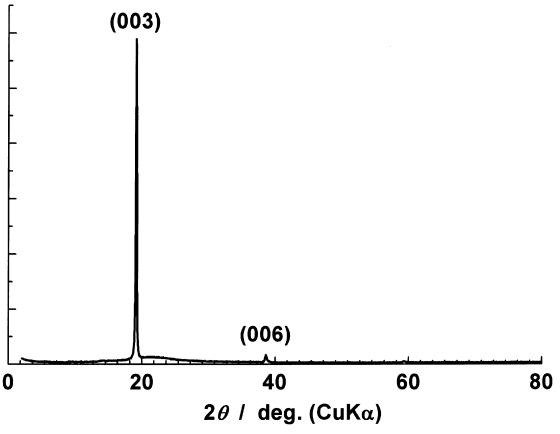

Fig. 1. XRD pattern of $LiCoO_2$ thin film deposited on quartz glass for 2 h.

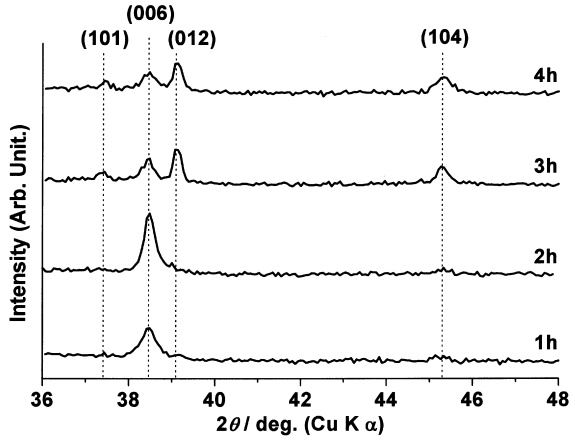

Fig. 2. XRD patterns in the 2θ range of 35–48° of $LiCoO_2$ thin films deposited on quartz glass for 1, 2, 3, and 4 h.

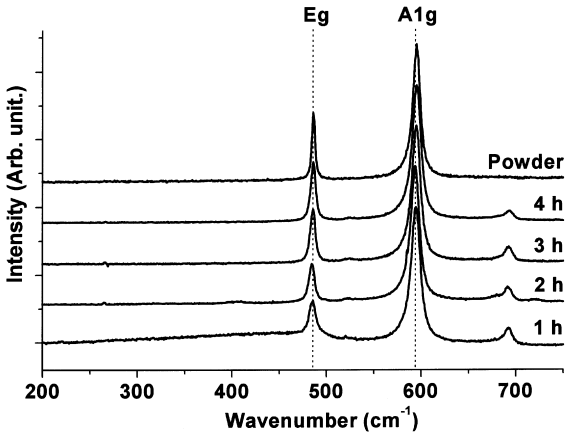

Fig. 3. Raman spectra of $LiCoO_2$ thin films deposited on quartz glass for 1, 2, 3, and 4 h and of a $LiCoO_2$ powder sample.

preferred *c*-axis [(0 0 3)] orientation to the substrate surface. Fig. 2 shows the variation of XRD patterns in the 2θ range of 35–48° of thin films deposited on quartz glass with changing deposition time. In each XRD pattern, the (0 0 3) line was observed with a high intensity (not shown in Fig. 2). The (0 0 6) reflection was the only peak in the 2θ range for the films deposited for 1 and 2 h, whereas three other peaks appeared at $2\theta = 37.40$, 39.09, and 45.29°, which are indexed as the (1 0 1), (0 1 2), and (1 0 4) reflections, after deposited for 3 and 4 h. The variation in Fig. 2 indicates that the degree of the *c*-axis orientation decreased with increasing deposition time, that is, with the thickness of the films. The thickness of the film estimated from SEM images was 0.12 μm for the film deposited for 1 h, and increased to 0.34 μm after deposition for 3 h. The deposition rate calculated from the thickness changes was about 2 nm min^{-1} (3 pm per pulse), which was much slower than that reported by Antaya et al. (about 400 nm min^{-1}) [14].

We tried to examine the preferred orientation of thin films deposited on polycrystalline Pt and Au substrates by XRD; however, we were not able to assign clearly the peaks in this 2θ range because of their quite low intensities and the interference from the large peaks of the substrates. Hence, we used Raman spectroscopy to examine the preferred orientation on Pt and Au substrates. $LiCoO_2$ exhibits two Raman bands at 486 (E_g mode) and 596 cm^{-1} (A_{1g} mode), and their relative intensities change with the degree of *c*-axis orientation [15]. Fig. 3 shows non-polarized Raman spectra of thin films deposited for 1–4 h on quartz glass substrates, together with a spectrum of $LiCoO_2$ powder as a reference. Each spectrum in Fig. 3 is normalized by the intensity of the A_{1g} peak at 596 cm^{-1}. A broad background in the range of 200–500 cm^{-1} observed in the spectrum for the film deposited for 1 h originated from the quartz glass substrate. In addition to the E_g and A_{1g} peaks, a small peak assigned to Co_3O_4 was observed at 690 cm^{-1} for each film. The presence of Co_3O_4 peak indicates that the films were slightly deficient in lithium. The powder sample exhibited the two bands with an intensity ratio I_{486}/I_{596} of about 0.5, where I_{486} and I_{596} are the intensities of the E_g and A_{1g} bands, respectively. The I_{486}/I_{596} ratios were 0.29, 0.30, 0.38, and 0.45 for the films deposited for 1, 2, 3, and 4 h, respectively, which indicated that the ratio increased with a decrease in the degree of the *c*-axis orientation of the films (Fig. 2). The film deposited for 4 h had a ratio close to that of the powder sample, indicating the film had practically no preferred orientation. The I_{486}/I_{596} ratios obtained for thin films deposited on different kinds of substrates for 1–4 h are summarized in Table 1. The I_{486}/I_{596} ratio was affected by deposition time, but did not depend on the kind of substrates. From the results listed in Table 1, it was confirmed that *c*-axis oriented films are obtained on Pt and Au substrates as well. Hereafter the *c*-axis oriented thin films are referred to as *c*-films, while the randomly oriented films as *r*-film.

The observed *c*-axis orientation that is independent of the kind of the substrates can be explained by the lowest surface energy of the (0 0 3) plane because it is the most closely packed plane of $LiCoO_2$, according to Braives's empirical law [20]. Bates et al reported that very thin $LiCoO_2$ films (0.1 μm or less) prepared by RF sputtering tend to have *c*-axis orientation [21]. The thicknesses of the *c*-axis

Table 1
Raman I_{486}/I_{596} ratios obtained for $LiCoO_2$ thin films deposited by PLD on different kinds of substrates for 1–4 h

Deposition time (h)	I_{486}/I_{596}[a]		
	Quartz glass	Pt	Au
1	0.29	0.27	0.29
2	0.30	–	0.33
3	0.38	0.40	0.42
4	0.45	–	0.44
Powder		∼0.50	

[a] I_{486}: the intensity of the E_g band; I_{596}: the intensity of the A_{1g} band.

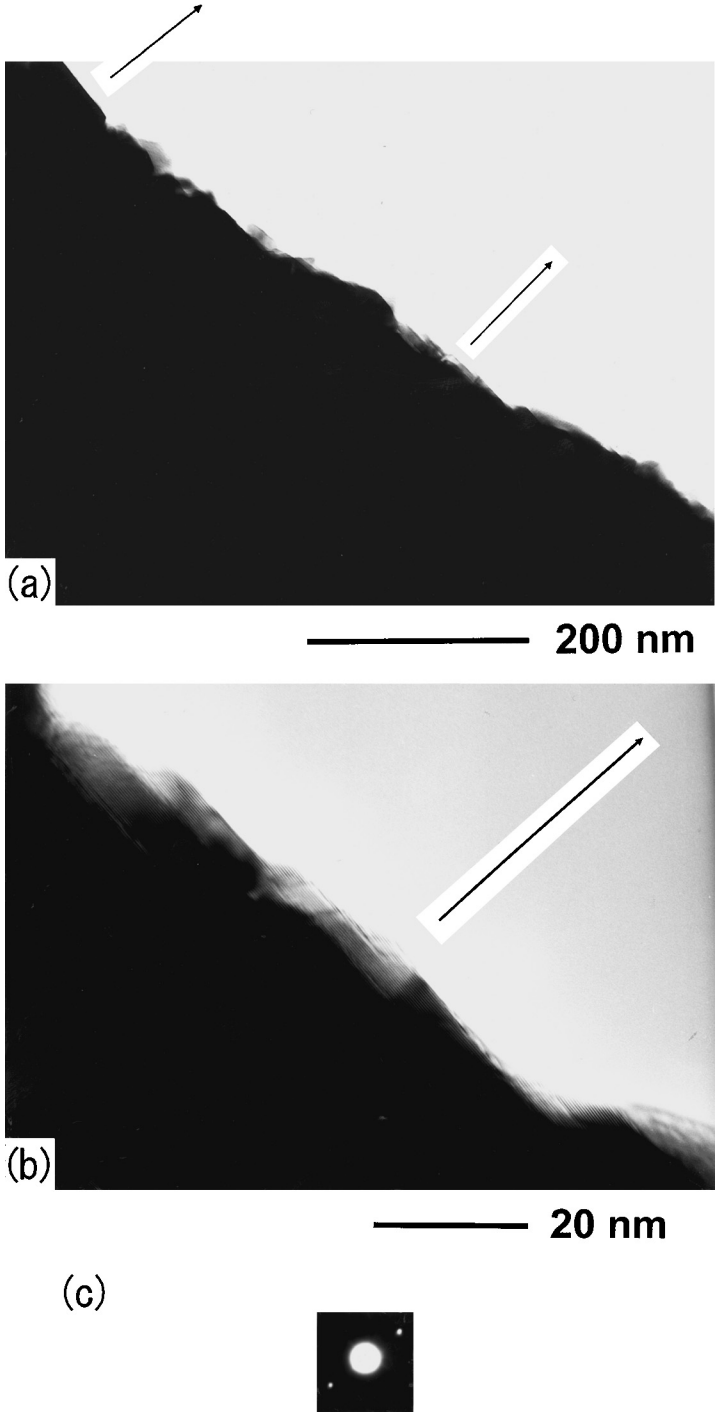

Fig. 4. (a) TEM image of *c*-axis oriented thin film of $LiCoO_2$ deposited on an Au micro grid for 1 h. Arrows show the directions of the *c*-axis of $LiCoO_2$. (b) Magnified image of (a). (c) Selected area electron diffraction pattern of (a).

oriented films obtained in the present study were thicker (up to 0.24 μm after deposited for 2 h) than their criterion, but the tendency was in agreement with their results.

Fig. 4(a) and (b) show TEM images of a *c*-film deposited for 1 h on Au micro grid. Fig. 4(b) shows a magnified image of Fig. 4(a). The selected area electron diffraction pattern of Fig. 4(a) is shown in Fig. 4(c). Arrows in Fig. 4(a) and (b) indicate the directions of the *c*-axes perpendicular to the (0 0 3) planes of the lattice images observed in these areas. The film had a smooth surface as shown in Fig. 4(a). In Fig. 4(b), the (0 0 3) planes are aligned parallel to the substrate surface. Similar lattice images were observed at many different parts of the film. The two arrows in Fig. 4(a) are nearly parallel to each other and normal to the substrate surface, which confirms that the film was *c*-axis oriented. The *c*-axis orientation of the film is also confirmed by the

selected area electron diffraction pattern in Fig. 4(c), in which diffraction spots from the (0 0 3) planes were observed only in a single direction. A closer look at Fig. 4(b) revealed that the *c*-film consisted of the (0 0 3) terraces separated by steps of different heights. The observed step-and-terrace structure of the film indicates that the growth rate of the film in the direction parallel to the (0 0 3) plane was faster than that in the direction normal to the plane. Crystal planes with a high atomic density such as the (0 0 3) planes generally need more atoms to grow than those with a low atomic density, so that the growth rate should be smaller.

A TEM image of an *r*-film deposited for 3 h on Au micro grid and its selected area electron diffraction pattern are shown in Fig. 5(a) and (b), respectively. The *r*-film consisted of grains of 40–70 nm in length, and its surface was fairly rough. In this area, three lattice images of the (0 0 3) planes were observed, but their *c*-axes were randomly oriented as shown by the arrows in Fig. 5(a). The selected area electron diffraction pattern showed visible diffraction spots from the (0 0 3) planes in four directions. These results confirm that the films deposited for 3 h consisted of randomly oriented grains of $LiCoO_2$ with many grain boundaries between them.

Lithium-ion transport plays an important role in the performance of the electrode. Considering the results of XRD, Raman spectroscopy, and TEM shown above, the difference in the orientation of the films should affect the transport of lithium ions during charging and discharging, because it is reasonable to expect from the $LiCoO_2$ lattice that lithium diffusion is fast in the direction parallel to the (0 0 3) plane, but is practically impossible in the direction normal to the plane. In addition, the surface of *r*-films is rougher than *c*-films. Hence the real surface area of the former is much larger than that of the latter, which will cause a significant difference in the rate of the charge-transfer reaction.

3.2. Electrochemical behavior of the c- and r-films at the initial stages

Fig. 6 shows cyclic voltammograms of thin films deposited for 1, 2, and 3 h on Pt substrates. As shown earlier, the films deposited for 1 and 2 h had *c*-axis orientation, while the

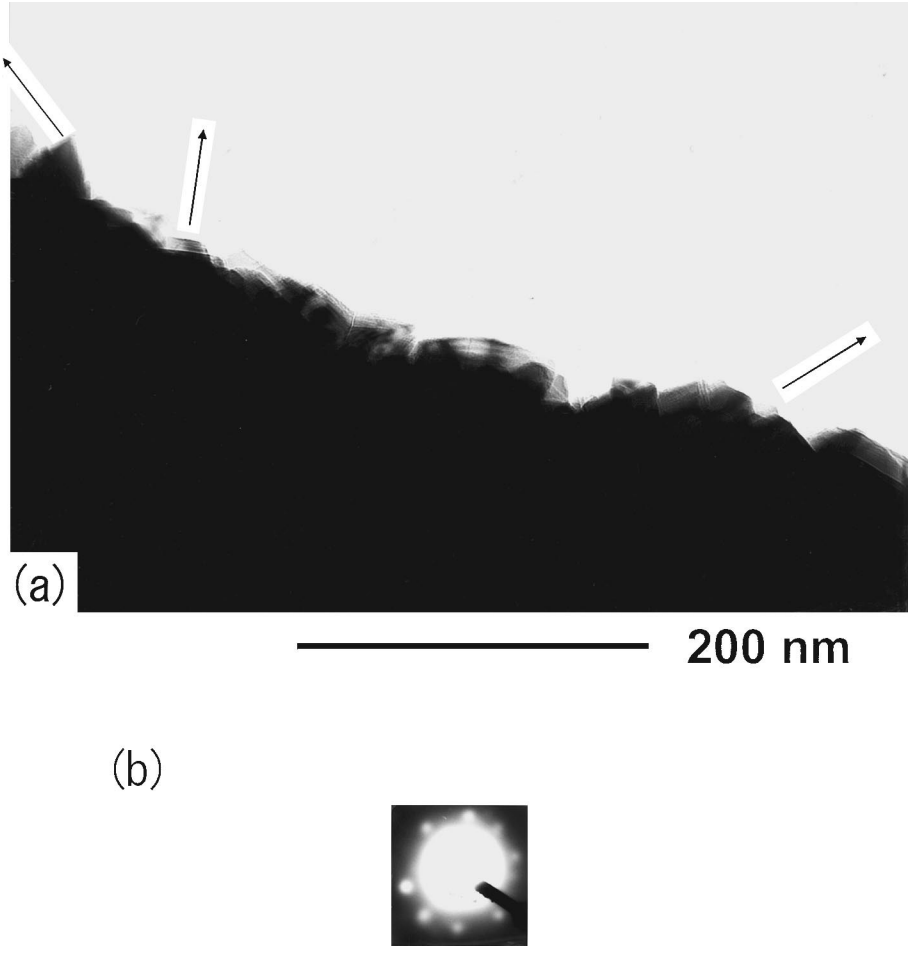

Fig. 5. (a) TEM image of randomly oriented thin film of $LiCoO_2$ deposited on an Au micro grid for 3 h. Arrows show the directions of the *c*-axis of $LiCoO_2$. (b) Selected area electron diffraction pattern of (a).

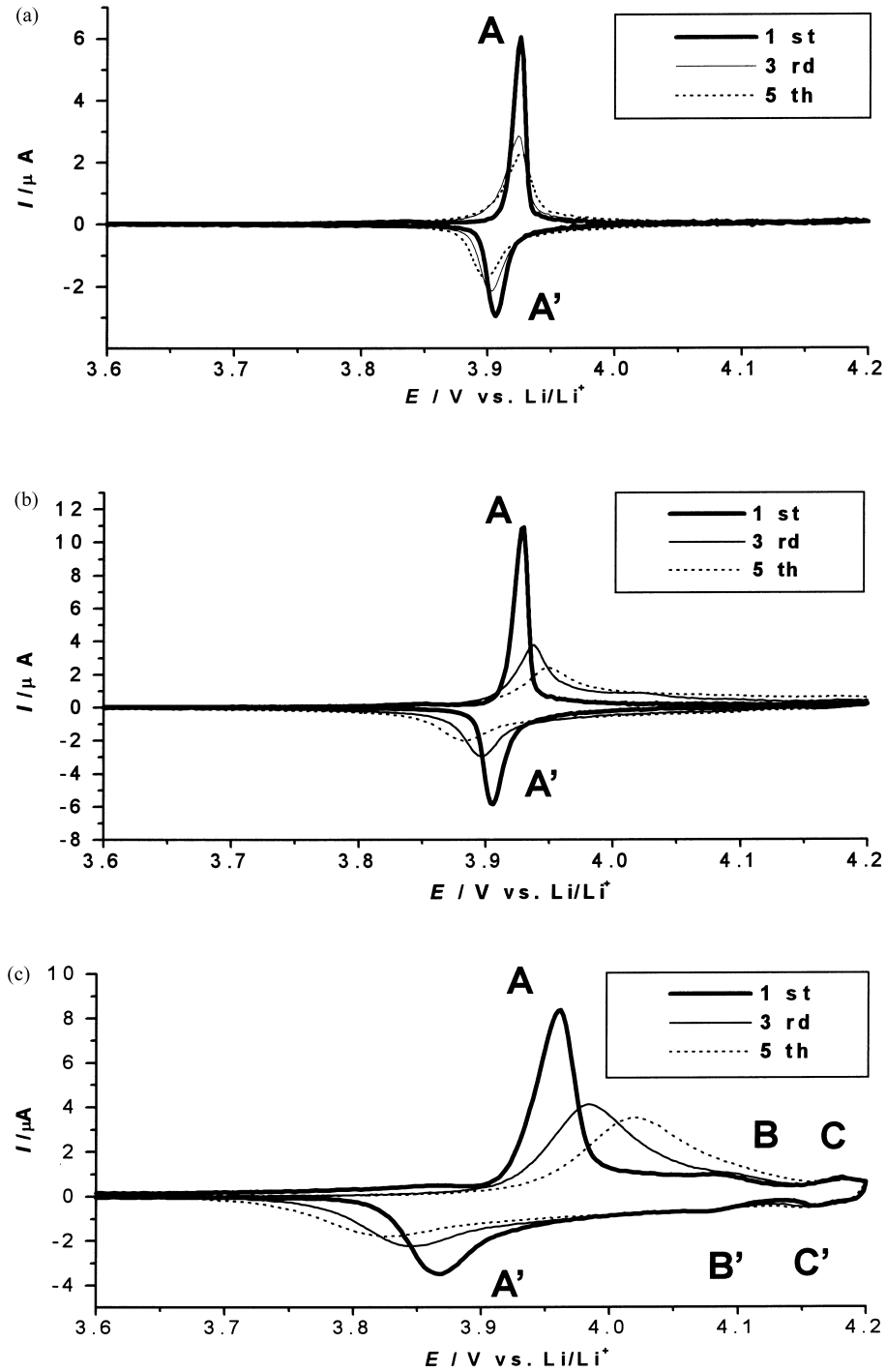

Fig. 6. Cyclic voltammograms of $LiCoO_2$ thin films deposited on Pt substrates (0.07 cm^2) for (a) 1; (b) 2 and (c) 3 h. $v = 0.1$ mV s^{-1}.

film deposited for 3 h had no preferred orientation. First we discuss their electrochemical behaviors in the first cycle. For each voltammogram, large anodic and cathodic peaks designated by A and A′, respectively, are seen at around 3.9 V. The couple are attributed to a first-order phase transition between two different hexagonal phases in the range of $0.93 \geq x \geq 0.75$ in Li_xCoO_2 (called the two-phase co-existence region) [3]. The peaks of the *c*-films were very sharp [full widths at half maximum (FWHMs) of the anodic peaks: 11 mV (1 h) and 13 mV (2 h)] and their peak separations were quite small (20 mV in both case), whereas the peaks of the *r*-film were broad [FWHM: 36 mV (3 h)] and their peak separation was large. The sharpness of peaks A and A′ of the *c*-films and their small peak separation can be explained by their thinner and more uniform texture than those of the *r*-films as shown in the previous section.

At potentials more positive than 4.0 V, lithium-ion extraction/insertion proceeds in the host of a single phase.

Order–disorder phase transitions from the hexagonal to a monoclinic phase and from the monoclinic to another hexagonal phase take place at 4.06 and 4.16 V, respectively [3], which are seen as small peaks designated by B and B′, and C and C′, respectively, in the voltammogram of the *r*-film shown in Fig. 6(c). The peaks corresponding to these order–disorder phase transitions did not appear in the first cycle of the *c*-films (Fig. 6(a) and (b)). The charging capacity between 3.6 and 4.0 V ($Q_{3.6–4.0V}$), which originates mainly from the two-phase regions, and the capacity between 4.0 and 4.2 V ($Q_{4.0–4.2\ V}$), which originates mainly from the single-phase region, were estimated by integrating the anodic current in Fig. 6. The calculated values of $Q_{4.0–4.2\ V}/Q_{3.6–4.0\ V}$ were 15, 17, and 41% for the films deposited for 1, 2, and 3 h, respectively, in the first cycle. The ratio for the *r*-film is very close to that estimated from charge–discharge curves for $LiCoO_2$ composite electrodes reported in the literature (43%) [3]. The capacity of the *c*-films at potentials more positive than 4.0 V was much smaller than that of the *r*-film or composite electrodes; that is, the reactivity of the *c*-films in the single-phase region was lower than that in the two-phase region.

In order to understand the difference in the electrochemical behaviors observed in the first cycle, ac impedance spectra of thin films were measured. The results for a *c*-film deposited for 1 h and an *r*-film deposited for 3 h on Au are shown in Fig. 7. The spectra were measured at 4.00 (first hexagonal), 4.10 (monoclinic), and 4.20 V (second hexagonal) in the single-phase region. Each spectrum consisted of a semicircle in the high frequency region (>20 Hz), which is assigned to charge-transfer impedance [22], and a straight line with a slope of 45° coupled with a nearly vertical line in the low frequency region (<20 Hz), which correspond to semi-infinite and finite-space diffusion, respectively. The semicircles in the high frequency region were fitted using a parallel equivalent circuit of the double layer capacitance (C_{dl}) and the charge-transfer resistance (R_{ct}). The calculated values of R_{ct} were 69 and 35 Ω at 4.0 V for the *c*- and *r*-films, respectively. Considering the results of the structural analysis in the previous section, the *r*-film should have a larger real surface area than the *c*-film. Hence, the larger real surface area of the *r*-film resulted in the observed smaller charge-transfer resistance.

As mentioned above, the vertical lines at the very low frequencies in Fig. 7(a) and (b) correspond to finite space diffusion. Both films are thin enough to obtain lithium diffusion coefficients using the following equation [22]

$$\tilde{D}_{Li} = \frac{l^2}{3R_L C_L} \quad (1)$$

where C_L is the limiting low frequency capacitance, R_L the limiting low frequency resistance, and l denotes the film thickness. It should be noted that $\tilde{D}_{Li}$ in Eq. (1) denotes the apparent diffusion coefficient in the direction normal to the substrate surface. The values of $\tilde{D}_{Li}$ at 4.0 V were

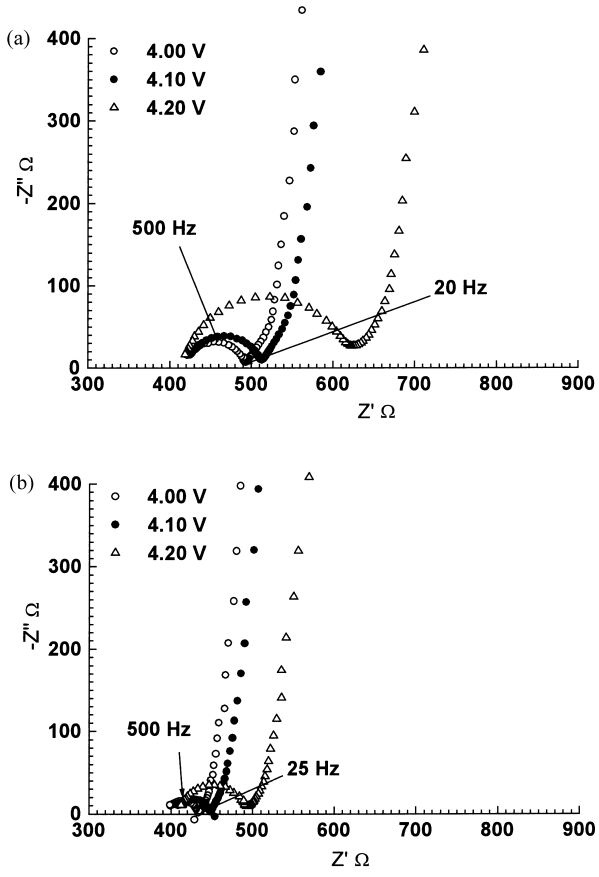

Fig. 7. AC impedance spectra at potentials of 4.0, 4.1, and 4.2 V, of $LiCoO_2$ thin films deposited on Au substrate (0.20 cm^2) for (a) 1 and (b) 3 h.

determined to be 1.2×10^{-11} and 5.0×10^{-10} $cm^2\ s^{-1}$ for the *c*- and *r*-films, respectively. The difference in $\tilde{D}_{Li}$ between the two films originates from to the difference in the texture discussed in the previous section.

3.3. Changes of electrochemical behavior upon repeated cycling

In the second and third cycles, the shape of the voltammograms changed significantly. The heights of peaks A and A′ decreased and their peak separation increased upon cycling in each case. Such tendency was most significantly observed for the *r*-film. The charging capacities were estimated by integrating the anodic current between 3.6 and 4.2 V, and the percentages of utilization of the active material were calculated from the film thickness, the electrode area, and the density of $LiCoO_2$ (5.05 g cm^{-3}) [3]. The results are shown in Table 2. The utilization of the *c*-film (deposited for 1 h) was only 55.7% and tended to increase slightly upon repeated cycling. The poor utilization of the *c*-film is attributed to the difficulty in the mass-transport of lithium ions in the direction normal to the (0 0 3) plane. The slight increase in the utilization upon cycling may be due to

Table 2
The utilization of the active material estimated from the integration of charging current between 3.6 and 4.2 V

Deposition time (h)	Utilization (%)				
	First cycle	Second cycle	Third cycle	Fourth cycle	Fifth cycle
1	55.7	49.1	51.8	53.8	56.3
3	101.2	86.2	84.6	82.7	81.1

micro-crack formation during charging and discharging, which would have enabled the inside of the film to be used.

On the other hand, the utilization of the *r*-film (deposited for 3 h) was over 80% except in the first cycle, and decreased upon repeated cycling. As was seen in Fig. 4, the film consisted of randomly oriented small grains with many grain boundaries, the texture of which is similar to that of composite electrodes made of the powder. The mass transport of lithium ions should be easier than that in the *c*-film, which resulted in high utilizations of the *r*-film. The decrease in the utilization upon cycling is probably because some grains were isolated by crack formation during charging and discharging. It was reported that the electronic conductivity of Li_xCoO_2 greatly changes with lithium content x, and is very low at $x \sim 1$ at potentials <3.9 V [23]. Once electronically isolated grains of $LiCoO_2$ are formed, they will not be able to participate again in the electrode reactions in the following cycles because no conductive additives are present in the film.

The observed increase in peak separation also resulted from a decrease in the uniformity of the film and an increase in inter-particle resistance caused by micro-crack formation. The peak separation of the *r*-film was more significant than that of the *c*-films. This fact indicates that the texture of the thin *c*-films consisting of well-aligned (0 0 3) planes is more stable against the volume changes during charging and discharging than the randomly oriented texture of the *r*-films.

4. Conclusions

Thin films of $LiCoO_2$ with a preferred *c*-axis orientation were prepared by PLD. Thin films deposited for 1–2 h had a preferred *c*-axis orientation, but films deposited for 3 h and longer lost the preferred orientation. The electrochemical properties were different between the *c*- and *r*-films. The anodic and cathodic peaks of the *c*-films corresponding to the first-order phase transition at around 3.9 V were sharp and their peak separation was small due to their thin and uniform structure. However, their smooth surface and texture consisting of aligned (0 0 3) planes gave larger R_{ct} and smaller $\tilde{D}_{Li}$ in the direction perpendicular to the surface, respectively. These features resulted in poor utilizations of the active material. On the other hand, the *r*-films exhibited nearly the same electrochemical behaviors as those of composite electrodes made of $LiCoO_2$ powder. The *r*-films consisted of small grains of 40–70 nm with many grain boundaries. The texture facilitated the mass-transport of lithium ions, and thus resulted in better utilizations of the active material.

Finally, the *c*-films showed an unexpected property, that is, the poor reactivity in the single-phase regions at potentials more positive than 4.0 V. Unfortunately, the reasons for this behavior remained unanswered in the present study. The poor reactivity in the single-phase region at potentials >4.0 V may be also caused by their unique texture, and is needed to be investigated further.

Acknowledgements

This work was supported by CREST of JST (Japan Science and Technology).

References

[1] K. Mizushima, P.C. Jones, P.J. Wiseman, J.B. Goodenough, Mater. Res. Bull. 15 (1980) 783.
[2] M.G.S.R. Thomas, P.G. Bruce, J.B. Goodenough, Solid State Ionics 17 (1985) 13.
[3] J.N. Reimers, J.R. Dahn, J. Electrochem. Soc. 139 (1992) 2091.
[4] T. Ohzuku, A. Ueda, J. Electrochem. Soc. 141 (1994) 2972.
[5] G.G. Amatucci, L.M. Tarascon, L.C. Klein, J. Electrochem. Soc. 143 (1996) 1114.
[6] M. Menetrier, I. Saadoune, S. Levasseur, C. Delmas, J. Mater. Chem. 9 (1999) 1135.
[7] I. Uchida, H. Sato, J. Electrochem. Soc. 142 (1995) L135.
[8] H. Sato, D. Takahashi, T. Nishina, I. Uchida, J. Power Sources 68 (1997) 540.
[9] B. Wang, J.B. Bates, F.X. Hart, B.C. Sales, R.A. Zuhr, J.D. Robertson, J. Electrochem. Soc. 143 (1996) 3203.
[10] J.B. Bates, N.J. Dudney, B.J. Neudecker, F.X. Hart, H.P. Jun, S.A. Hackney, J. Electrochem. Soc. 147 (2000) 59.
[11] B. Roas, L. Schultz, G. Endres, Appl. Phys. Lett. 53 (1988) 1557.
[12] C.W. Nieh, L. Anthiny, J.Y. Josefowicz, F.G. Krajenbrink, Appl. Phys. Lett. 56 (1990) 2138.
[13] C. Belouet, Appl. Surf. Sci. 96/98 (1996) 630.
[14] M. Antaya, K. Cearns, J.S. Preston, J.N. Reamers, J.R. Dahn, J. Appl. Phys. 76 (1994) 2799.
[15] M. Inaba, Y. Iriyama, Z. Ogumi, Y. Todzuka, A. Tasaka, J. Raman Spectrosc. 28 (1997) 613.
[16] A. Masuda, K. Matsuda, Y. Tonezawa, A. Morimoto, T. Shimizu, Jpn. J. Appl. Phys. 35 (1996) L234.
[17] O. Eryu, K. Murakami, K. Masuda, K. Shihoyama, T. Mochizuki, Jpn. J. Appl. Phys. 31 (1992) L86.
[18] M. Haruna, H. Ishizuki, J. Tsutsumi, Y. Shimaoka, H. Nishihara, Jpn. J. Appl. Phys. 34 (1995) 6084.
[19] Y. Iriyama, M. Inaba, T. Abe, Z. Ogumi, Solid State Ionics, in press.
[20] K. Wasa, S. Hayakawa, Hakumakuka Gijyutu (Thin Film Technology), Kyoritsu-Syuppan, Tokyo, 1982, p. 66 (in Japanese).
[21] F.X. Hart, J.B. Bates, J. Appl. Phys. 83 (1998) 7560.
[22] C. Ho, I.D. Raistrick, R.A. Huggins, J. Electrochem. Soc. 127 (1980) 3.
[23] M. Shibuya, T. Nishina, T. Matsue, I. Uchida, J. Electrochem. Soc. 143 (1996) 3157.